Symmetry consideration in zero loop-area Sagnac interferometry at oblique incidence for detecting magneto-optic Kerr effects

X. D. Zhu

Citation: Review of Scientific Instruments **88**, 083112 (2017); doi: 10.1063/1.4990669
View online: http://dx.doi.org/10.1063/1.4990669
View Table of Contents: http://aip.scitation.org/toc/rsi/88/8
Published by the American Institute of Physics

Symmetry consideration in zero loop-area Sagnac interferometry at *oblique incidence* for detecting magneto-optic Kerr effects

X. D. Zhu[a)]
Department of Physics, University of California, Davis, California 95616, USA

(Received 16 June 2017; accepted 3 August 2017; published online 22 August 2017)

I present a detailed account of a zero loop-area Sagnac interferometer operated at *oblique incidence* for detecting magneto-optic Kerr effects arising from a magnetized sample. In particular, I describe the symmetry consideration and various optical arrangements available to such an interferometer that enables measurements of magneto-optic effects due to both in-plane and out-of-plane magnetization of the sample with optimizable signal-to-noise ratios. *Published by AIP Publishing.* [http://dx.doi.org/10.1063/1.4990669]

I. INTRODUCTION

Intrinsic magnetic ordering and responses to externally applied fields (electric as well as magnetic) are among the most important characteristics of materials, whether in gas phase, liquid phase, or solid phase.[1–3] One important class of experimental methods for studying such magnetic properties of a material is based on the optical response to the magnetization in the material.[4–6] The latter alters the polarization state of a reflected (Kerr effect) and transmitted (Faraday effect) optical beam through dielectric tensor elements induced by the magnetization. Though not as sensitive as SQUID-based methods that directly measure the magnetization in a sample, optical methods have the advantage of being non-intrusive, versatile, and applicable over a wide range of experimental conditions, and being a local probe to the magnetic property only from the illuminated region of the sample.

In practice, linear birefringence is ubiquitous, particularly in elements of an optical detection system. In this study, I will refer birefringence as linear dielectric responses of uniaxial materials, biaxial materials, and optically active and dichroic materials that preserve time reversal symmetry. I will separately consider linear magneto-optic responses of materials that break time-reversal symmetry, even though the magneto-optical responses also cause birefringence. Because the optical response to birefringence is orders of magnitude larger than the magneto-optic response, even residual birefringence readily produces an overwhelming effect on the polarization state of an optical beam. As a result, magneto-optic measurements are typically done by modulating the magnetization and detecting corresponding changes in the polarization state of the optical beam with phase-sensitive or equivalent methods. Modulation-based detection has enabled measurements of Kerr rotation (in reflection geometry) and Faraday rotation (in transmission geometry) as small as 10^{-7} rad.[7] When repeatedly altering the sample magnetization for measurement is not an option, the effect of birefringence can still be removed if one takes advantage that the magneto-optic effect breaks time-reversal symmetry (TRS) while the birefringence maintains TRS.[8–10] As shown by Spielman and co-workers, a Sagnac interferometry is just such an optical detection system that measures the time-reversal-symmetry-breaking (TRSB) effect while suppressing effects that observe TRS. In such an interferometer, an optical beam and its time-reversal counterpart traverse an identical loop-wise path but in the opposite direction. One measures the difference of the phases acquired by these two beams. The birefringence in the loop produces a reciprocal (*direction-independent*) phase that is common to both beams. As a result, the birefringence effect is removed in the differential phase by symmetry. If the optical path includes reflection from and/or transmission through a magnetized sample, the magneto-optic effect yields a non-reciprocal (*direction-dependent*) phase in the two beams that have the same amplitude but opposite signs. Consequently the magneto-optic effect that breaks TRS is doubled in the differential phase instead. The Sagnac interferometer measures this differential phase.

If the loop-wise path in a Sagnac interferometer (i.e., the Sagnac loop) encloses a finite area, time-reversal symmetry breaking effects can have a contribution from the Doppler's effect when the loop as a whole also executes a rotational motion or a combination of rotational motions. If the loop-wise optical path encloses no area (also known as "loopless" or zero loop-area), time-reversal symmetry breaking effects only come from materials that the beams traverse through or reflect off. For a finite loop-area Sagnac interferometer, optical beams are produced through beam-splitting optical elements and can be configured to be either normally or obliquely incident on a sample so that effects of magnetization parallel as well as perpendicular to the sample surface can be measured. Because the two counter-propagating beams are controlled separately and need to be recombined eventually before detection, extra optical elements are needed. These elements are introduced in ways that are difficult to maintain the two counter-propagating beams exactly along the same Sagnac loop, making a finite loop-area interferometer more readily subject to residual misalignments and mechanical drifts in the interferometer including the sample. This has so far limited its sensitivity for Kerr rotation measurement to 1×10^{-6} rad.[8,9,11] For a zero loop-area Sagnac interferometer,

a)Email: xdzhu@physics.ucdavis.edu

two counter-propagating beams are two orthogonally polarized components of the single optical beam, and thus one does not need beam splitting and beam recombination for operation. As a result, significantly fewer optics are needed, and the interferometer can be arranged to minimize effects of misalignment and mechanical drifts. It has been shown by Xia *et al.* and Fried *et al.* that such a zero-area Sagnac interferometer can detect Kerr rotation as small as 10^{-7} rad without modulating magnetization.[12–14]

We recently developed an oblique-incidence zero loop-area Sagnac interferometer (OI ZA-SI) in which the optical beams interact with a magnetized sample at oblique incidence so that effects of in-plane magnetization, namely, longitudinal and transverse Kerr effects, can be measured.[15] In this paper, I present symmetry considerations in such an interferometer. Some of the symmetry properties are common to all forms of Sagnac interferometers.[15,16] Others are available only to the interferometers at oblique-incidence. Through symmetry consideration, I show that the arrangement of the oblique-incidence zero loop-area Sagnac interferometer can be individually optimized to detect components of magnetization in a sample.

II. OBLIQUE-INCIDENCE ZERO LOOP-AREA SAGNAC INTERFEROMETER (OI ZA-SI)

An arrangement of such an interferometer is shown in Fig. 1. A broad-band source is collimated and passes through a beam splitter and a linear polarizer (PL) with the transmission axis (TA) aligned parallel to the slow axis (SA) of a 1-m polarization-maintaining (PM) fiber. The SA of the fiber bisects the transverse magnetic TM axis and the transverse electric (TE) axis of an electro-optic modulator (EOM) that adds a time-dependent phase to the TM mode. The beam after EOM is coupled into a 10-m PM fiber with the TM axis aligned to the SA axis of the fiber. The SA of the 10-m PM fiber at the output end is aligned parallel to the p-polarization with respect to the sample. The optical beam emerging from the 10-m fiber diverges and is thus collimated with a 10× objective and passes through a wave plate (Wave plate #1). Up to this point, the arrangement is in essence same as a normal-incidence zero loop-area Sagnac interferometer (NI ZA-SI).[12,13] It is to prepare two orthogonally polarized components from a single optical beam with the short coherent length (in the order of 20–30 μm), add a time-dependent phase $\Phi(t) = \Phi_0 \cos(2\pi ft) = \Phi_0 \cos(\Omega t)$ to each of them but at a delayed time τ, recombine the two components when they return, and send the recombined beam to a photo-receiver (by the beam splitter) for the Fourier analysis to yield the differential phase. The differential phase reveals the time-reversal symmetry breaking effect in the optical path beyond this portion of the interferometer. The second portion of the interferometer differs from a normal-incidence interferometer, most notably the oblique incidence at the sample and a reflection mirror that sends the beam back to complete the Sagnac loop without enclosing a loop area. These differences enable such a zero loop-area Sagnac interferometer to detect in-plane as well as out-of-plane components of the magnetization in a magnetized sample. From symmetry considerations as I will outline next, an OI ZA-SI enables different arrangements such that one can choose one that yields the magneto-optic response from a Cartesian component of the sample magnetization with the highest available signal-to-noise ratio.

Before going into symmetry considerations, we revisit the Jones vectors for orthogonally polarized components for an optical beam and Jones matrices for optical elements including a magnetized sample in an interferometer. Symmetry considerations will be discussed on the basis of these Jones matrices and Jones vectors. Let $P_{10} = \begin{bmatrix} 1 \\ 0 \end{bmatrix}$ and $P_{20} = \begin{bmatrix} 0 \\ 1 \end{bmatrix}$ be two linearly polarized components of the broadband optical beam emerging from the 10-m PM fiber: one is aligned along the SA of the PM fiber (i.e., the p-polarization with respect to the sample), and the other is aligned along the fast axis (FA) of the fiber (i.e., the s-polarization with respect to the sample). We produce two orthogonally polarized components $P_1 = \begin{bmatrix} a \\ be^{i\varphi} \end{bmatrix}$

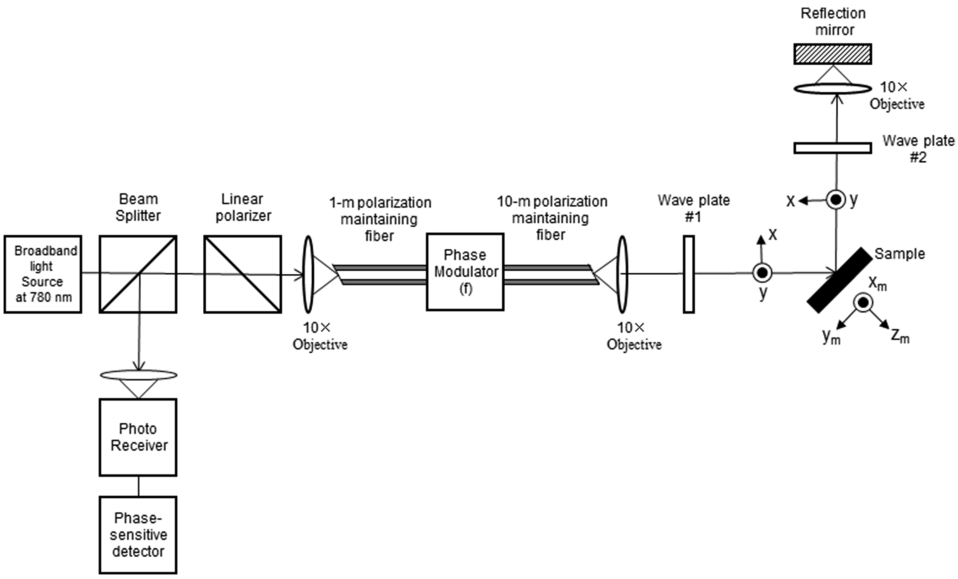

FIG. 1. An arrangement of a zero loop-area Sagnac interferometer for measuring longitudinal and polar Kerr effects of a magnetized sample. The TA of the linear polarizer is aligned to the SA of the 1-m PM fiber. The latter bisects TM and TE axes of the electro-optic phase modulator (EOM). The SA of the 10-m PM fiber is aligned to the TM axis of EOM and parallel to the x-axis before the sample. Wave plate #1 is set to produce $P_1 = \begin{bmatrix} a \\ be^{i\varphi} \end{bmatrix}$ and $P_2 = \begin{bmatrix} b \\ -ae^{i\varphi} \end{bmatrix}$ (with $\sqrt{a^2 + b^2} = 1$) from $P_{10} = \begin{bmatrix} 1 \\ 0 \end{bmatrix}$ and $P_{20} = \begin{bmatrix} 0 \\ 1 \end{bmatrix}$. A portion of the returned beam is directed to a photo-receiver with the beam splitter, and the photocurrent is analyzed with a phase-sensitive detector.

and $P_2 = \begin{bmatrix} b \\ -ae^{i\varphi} \end{bmatrix}$ (with $\sqrt{a^2+b^2}=1$) before they are obliquely incident on the sample from $P_{10} = \begin{bmatrix} 1 \\ 0 \end{bmatrix}$ and $P_{20} = \begin{bmatrix} 0 \\ 1 \end{bmatrix}$ using a suitable wave-plate. P_1 and P_2 are the initial states of the two "counter-propagating beams." Let

$$M = \begin{bmatrix} m_{11} & m_{12} \\ m_{21} & m_{22} \end{bmatrix} \tag{1}$$

be the Jones matrix that represents the effect of all optical elements encountered by the "beams" as they traverse to the sample and eventually return after the second reflection from the sample. The matric elements include terms that vary linearly with three Cartesian components of the sample magnetization. The differential phase detected by the interferometer is given by[16]

$$\alpha_K = 2\theta_K = Arg\left\{\frac{P_2^\dagger M P_1}{P_1^\dagger M P_2}\right\} = Arg\left\{\frac{\left[ab\left(m_{11}-m_{22}e^{i2\varphi}\right)+\left(b^2-a^2\right)(m_{21}+m_{12})\,e^{i\varphi}/2\right]-(m_{21}-m_{12})\,e^{i\varphi}/2}{\left[ab\left(m_{11}-m_{22}e^{i2\varphi}\right)+\left(b^2-a^2\right)(m_{21}+m_{12})\,e^{i\varphi}/2\right]+(m_{21}-m_{12})\,e^{i\varphi}/2}\right\}, \tag{2}$$

where θ_K is customarily defined as the Kerr rotation. If the time reversal symmetry holds for all optical elements including the sample, we have $m_{12} = m_{21}$ from a general consideration (as I will elaborate in Sec. III) and $\alpha_K = 0$. If the time reversal symmetry is broken, we expect $m_{12} \neq m_{21}$ and the Kerr rotation $\alpha_K \neq 0$. To measure α_K, it is easily shown that the first two harmonics of EOM modulation frequency Ω obtained from the Fourier analysis of the photocurrent produced in the receiver are

$$I(\Omega) \cong (\gamma/2)\, I_{inc}\left|P_2^\dagger M P_1\right|^2 J_1(2\Phi_0)\,\alpha_K = (\gamma/2)\, I_{inc}\left|ab\left(m_{11}-m_{22}e^{i2\varphi}\right)+\left(b^2-a^2\right)(m_{21}+m_{12})\,e^{i\varphi}/2\right|^2 J_1(2\Phi_0)\,\alpha_K, \tag{3a}$$

$$I(2\Omega) \cong (\gamma/2)\, I_{inc}\left|P_2^\dagger M P_1\right|^2 J_2(2\Phi_0) = (\gamma/2)\, I_{inc}\left|ab\left(m_{11}-m_{22}e^{i2\varphi}\right)+\left(b^2-a^2\right)(m_{21}+m_{12})\,e^{i\varphi}/2\right|^2 J_2(2\Phi_0), \tag{3b}$$

where Ω (rad/s) is the angular frequency of the time-dependent phase $\Phi(t)$. It is set such that $\Omega\tau = \pi$ and thus extra time-dependent phases added to the two "counter-propagating beams" are $\Phi(t) = \pm\Phi_0\cos(\Omega t)$, –equal in magnitude and yet opposite in sign. I_{inc} is the power of the light source right before entering the beam splitter. γ is the overall throughput factor due to passing through the beam splitter, the linear polarizer, collimation and focusing lenses (objectives), the PM fiber-EOM-PM fiber assembly, and reflection off the sample twice. $J_1(x)$ and $J_2(x)$ are the Bessel functions. From measured values of $I(\Omega)$ and $I(2\Omega)$, one can deduce the differential phase

$$\alpha_K = \frac{I(\Omega)}{I(2\Omega)}\frac{J_2(2\Phi_0)}{J_1(2\Phi_0)}, \tag{4}$$

where α_K is a linear function of the Cartesian components of the sample magnetization and contributions to α_K from these components depend upon choices of $P_1 = \begin{bmatrix} a \\ be^{i\varphi} \end{bmatrix}$ and $P_2 = \begin{bmatrix} b \\ -ae^{i\varphi} \end{bmatrix}$, reflectivity coefficients of the sample, and optical elements after the sample through the Jones matrix in Eq. (1). The polar Kerr effect refers to the contribution from the z_m component of the magnetization (see Fig. 1); the longitudinal Kerr effect refers to the contribution from the y_m component of the magnetization, and transverse Kerr effect refers to the contribution from the x_m component of the magnetization. Since components of the sample magnetization transform differently under crystal symmetry operations, one should be able to choose P_1 and P_2 and optical elements after the sample so that the magneto-optic effect associated with a particular component is predominant.

In Sec. III, I will discuss symmetry considerations in deciding on $P_1 = \begin{bmatrix} a \\ be^{i\varphi} \end{bmatrix}$ and $P_2 = \begin{bmatrix} b \\ -ae^{i\varphi} \end{bmatrix}$ and optical elements after the sample. These considerations enable finding arrangements in an OI ZA-SI that detect the magneto-optic effect from each of the three Cartesian components of the sample magnetization with the highest available signal-to-noise ratios. Specifically, I will explore symmetry-based choices that maximize the product of $|ab(m_{11}-m_{22}e^{i2\varphi})+[(b^2-a^2)(m_{21}+m_{12})e^{i\varphi}]/2|^2$ and α_K in Eqs. (3a) and (3b).

III. CONSTRAINTS OF SYMMETRY OPERATION ON MAGNETO-OPTICAL RESPONSES IN AN OI ZA-SI

A. Time reversal symmetry (TRS) on Jones matrices of optical elements

We first examine properties of Jones matrices of optical elements including the sample in an OI ZA-SI system. Since the time reversal symmetry may be broken, for each optical element, we need to distinguish the Jones matrix for the forward-traveling beam from the matrix for the backward-traveling beam. We adopt the convention used by Kapitulnik *et al.*[11] for the x-y frame in which the Jones vector for the polarization state of a light beam is defined, and the convention used by Dodge *et al.*[16] for the x_m-y_m-z_m frame in which the components of the magnetization in a sample are expressed as shown in Fig. 1. Generally for any optical element in the interferometer including the sample, we can write down Jones matrices for a forward-propagating beam and a backward-propagating beam as

$$M^{(f)} = \begin{bmatrix} f_{11} & f_{12} \\ f_{21} & f_{22} \end{bmatrix}, \tag{5}$$

$$M^{(b)} = \begin{bmatrix} b_{11} & b_{12} \\ b_{21} & b_{22} \end{bmatrix}. \tag{6}$$

If the optical element preserves the time-reversal symmetry (TRS), it is easy to see that TRS requires

$$f_{11} = b_{11}, \tag{7a}$$
$$f_{22} = b_{22}, \tag{7b}$$
$$f_{12} = b_{21}, \tag{7c}$$
$$f_{21} = b_{12}. \tag{7d}$$

For a sequence of optical elements that preserve TRS, it is as easy to show that Eqs. (7) hold for the forward-propagating and the backward-propagating beams through these elements as a whole. Since *for a zero loop-area Sagnac interferometer, Jones matrices for the forward-propagating beam and the backward-propagating beam are the same and are given by* Eq. (1), TRS requires $m_{12} = m_{21}$ in Eq. (1). From Eq. (2), the differential phase α_K vanishes in this case.

If an optical element such as a magnetized sample breaks TRS, Eqs. (7a)–(7d) no longer hold in general. Such an element gives rise to a Faraday effect (if a transmitting optical element breaks TRS) or a Kerr effect (if a reflecting optical element breaks TRS). For example, the reflection matrix of a magnetized sample for a forward-propagating beam is[11,16]

$$M_R^{(f)} = \begin{bmatrix} r_p + \alpha_x m_x & \alpha_y m_y + \alpha_z m_z \\ -\alpha_y m_y + \alpha_z m_z & r_s \end{bmatrix}. \tag{8}$$

For a backward-propagating beam, the reflection matrix of the sample is

$$M_R^{(b)} = \begin{bmatrix} r_p - \alpha_x m_x & \alpha_y m_y - \alpha_z m_z \\ -\alpha_y m_y - \alpha_z m_z & r_s \end{bmatrix}. \tag{9}$$

When at least one of the three Cartesian components (m_x, m_y, m_z) of the sample magnetization is non-zero, we expect $m_{12} \neq m_{21}$ for the Jones matrix in Eq. (1) and a non-zero differential phase α_K emerges.

In practice, imperfections in optical elements and alignments are inevitable and seem poised to complicate the description so far. Fortunately these "imperfections" can be represented by a combination of "unaccounted" elements such as wave-plates, rotators, and linear polarizers. As long as these elements preserve TRS, their effects only change relative contributions by components of the sample magnetization to α_K and vanish if the sample is not magnetized.

B. Crystal symmetries on magneto-optic responses in different optical arrangements

We now consider the effect of crystal symmetries on the magnet-optic response[17] and how it enables one to measure the Kerr rotation due to each Cartesian component of the sample magnetization with the optimal signal-to-noise ratio. Similar to the account offered by Dodge *et al.*[16] on the crystal symmetry effect on magneto-optic responses in a finite-area Sagnac interferometer, we concern ourselves with orthogonally polarized beams $P_1 = \begin{bmatrix} a \\ be^{i\varphi} \end{bmatrix}$ and $P_2 = \begin{bmatrix} b \\ -ae^{i\varphi} \end{bmatrix}$ that transform into one another under the operation of a crystal symmetry such as C_2 and σ_v or a combination of the two that maps the source plane of the forward-traveling beam to the source plane of the backward-traveling beam after either one reflection or two reflections from the sample. If a component of the magnetization changes under the operation, such a component will contribute to α_K, otherwise α_K contains no contribution for the component. If there are more than one pair of orthogonally polarized beams (i.e., different choices of a, b, and φ) that transform into one another under the same symmetry operation or for the same polarization pair, there are more than one optical arrangement after the sample that keep the symmetry operation, the contribution from a sample magnetization component to α_K is expected to be different from one pair to another or from one arrangement to another. This affords the option to detect the Kerr effect from such a magnetization component with the highest available signal-to-noise ratio.

For a normal-incidence ZA-SI, the symmetry that maps the source of the forward-traveling beam onto the source of the backward-traveling beam and at the same time changes the z_m component of the sample magnetization (a pseudovector) is the reflection through the y_m-z_m plane (σ_v') followed by the reflection through the x_m-z_m plane (σ_v)—the *mm* operation. The only choice of the orthogonally polarized beams is $P_1 = \frac{1}{\sqrt{2}}\begin{bmatrix} 1 \\ e^{i\varphi} \end{bmatrix}$ and $P_2 = \frac{1}{\sqrt{2}}\begin{bmatrix} 1 \\ -1e^{i\varphi} \end{bmatrix}$ with $P_1 = mmP_2$ and $P_2 = mmP_1$. In this case, the Jones matrix M is simply the reflection matrix for the forward-traveling beam with $m_{11} = m_{22} = r_p = r_s \equiv r_n$ and $m_{12} = -m_{21} = \alpha_z m_z$. As a result, one only measures the polar Kerr rotation given by

$$\alpha_K \cong \frac{1}{\sin\varphi} \times \mathrm{Re}\left\{\left(-\frac{2\alpha_z m_z}{r_n}\right)\right\}, \tag{10}$$

$$I(\Omega) \sim |r_n|^2 \sin\varphi \times \mathrm{Re}\left\{\left(-\frac{2\alpha_z m_z}{r_n}\right)\right\}. \tag{11}$$

The parameter choice of P_1 and P_2 that maximizes $I(\Omega)$ or the signal-to-noise ratio is $\varphi = \pi/2$. These were the choice used by Xia *et al.* and Fried *et al.*[12,13]

We note that crystal symmetries considered by Dodge *et al.*[16] apply to finite-area Sagnac interferometers when two counter-propagating beams reflect off a magnetized sample only once and the Jones matrices for forward-traveling and backward-traveling beams are simply the corresponding reflection matrices given by Eqs. (8) and (9). For an oblique-incidence zero loop-area Sagnac interferometer, the Jones matrix in Eq. (1) includes effects of reflection twice off the sample from the opposite directions and effects of extra optical elements after the sample. And it is the same for both the forward-traveling and backward traveling beams. As a result, crystal symmetry operations that map the source of the forward-traveling beam to the source of the backward-traveling beam are $\sigma_v C_2 = C_2 \sigma_v$ and σ_v'. Under the operation of either one of them, m_y and m_z change signs while m_x remains unchanged.

Pairs of orthogonally polarized states that transform into one another under the operation of $\sigma_v C_2 = C_2 \sigma_v$ or σ_v' are $P_1 = \frac{1}{\sqrt{2}}\begin{bmatrix} 1 \\ e^{i\varphi} \end{bmatrix}$ and $P_2 = \frac{1}{\sqrt{2}}\begin{bmatrix} 1 \\ -e^{i\varphi} \end{bmatrix}$, namely, $P_1 = \sigma_v C_2 P_2 = \sigma_v' P_2$. If the optical elements after the sample remain unchanged under

the same operation, we only need to consider the effect of the symmetry operation on the components of the magnetization. This means that the Kerr rotation θ_K or the differential phase α_K only has contributions from m_y and m_z (longitudinal Kerr and polar Kerr effect),

$$\alpha_K = Arg\left\{\frac{\left(m_{11}-m_{22}e^{i2\varphi}\right)-\left(m_{21}-m_{12}\right)e^{i\varphi}}{\left(m_{11}-m_{22}e^{i2\varphi}\right)+\left(m_{21}-m_{12}\right)e^{i\varphi}}\right\}, \quad (12)$$

$$I(\Omega) \sim \frac{1}{4}\left|\left(m_{11}-m_{22}e^{i2\varphi}\right)\right|^2 \times Arg\left\{\frac{\left(m_{11}-m_{22}e^{i2\varphi}\right)-\left(m_{21}-m_{12}\right)e^{i\varphi}}{\left(m_{11}-m_{22}e^{i2\varphi}\right)+\left(m_{21}-m_{12}\right)e^{i\varphi}}\right\}. \quad (13)$$

For example, if there is no extra optical element after the sample except for the reflection mirror at normal incidence, we have

$$M = -\begin{bmatrix} r_p^2 & \alpha_y m_y\left(r_p+r_s\right)+\alpha_z m_z\left(r_p-r_s\right) \\ -\alpha_y m_y\left(r_p+r_s\right)-\alpha_z m_z\left(r_p-r_s\right) & r_s^2 \end{bmatrix}. \quad (14)$$

The differential phase only has contributions from longitudinal and polar Kerr effects,

$$\alpha_K = \mathrm{Im}\left\{\frac{4\left(\alpha_y m_y(r_p+r_s)+\alpha_z m_z(r_p-r_s)\right)e^{i\varphi}}{\left(r_p^2-r_s^2e^{i2\varphi}\right)}\right\}, \quad (15)$$

$$I(\Omega) \sim \left|\left(r_p^2-r_s^2e^{i2\varphi}\right)\right| \times \left|\left(\alpha_y m_y(r_p+r_s)+\alpha_z m_z(r_p-r_s)\right)e^{i\varphi}\right|. \quad (16)$$

In this arrangement, one is best served to measure the Kerr effect for the magnetization component that has the larger of $|r_p+r_s|$ and $|r_p-r_s|$. The measurement is further optimized by choosing φ that maximizes $\left|\left(r_p^2-r_s^2e^{i2\varphi}\right)\right|$. For example, for most opaque materials such as Ni, Co, and Fe, the reflectivity coefficients for p- and s-polarization have opposite signs and thus $|r_p-r_s|<|r_p+r_s|$. In this case, this geometry is best for measuring the polar Kerr effect. One can further choose $\varphi=\pi/2$ to maximize $\left|\left(r_p^2-r_s^2e^{i2\varphi}\right)\right|$.

If we add a quarter-wave plate (Wave plate #2 in Fig. 1) with the fast axis along the y-axis, this element remains unchanged under the operation of $\sigma_v C_2 = C_2\sigma_v$ or σ_v'. In this case,

$$M = \begin{bmatrix} r_p^2 & \alpha_y m_y\left(r_p-r_s\right)+\alpha_z m_z\left(r_p+r_s\right) \\ -\alpha_y m_y\left(r_p-r_s\right)-\alpha_z m_z\left(r_p+r_s\right) & -r_s^2 \end{bmatrix}, \quad (17)$$

$$\alpha_K = \mathrm{Im}\left\{\frac{4\left(\alpha_y m_y(r_p-r_s)+\alpha_z m_z(r_p+r_s)\right)e^{i\varphi}}{\left(r_p^2+r_s^2e^{i2\varphi}\right)}\right\}, \quad (18)$$

$$I(\Omega) \sim \left|\left(r_p^2+r_s^2e^{i2\varphi}\right)\right| \times \left|\left(\alpha_y m_y(r_p-r_s)+\alpha_z m_z(r_p+r_s)\right)e^{i\varphi}\right|. \quad (19)$$

In this arrangement, one is best served to measure the longitudinal Kerr effect for opaque materials as $|r_p-r_s|<|r_p+r_s|$. The measurement is further optimized by choosing $\varphi=0$ that maximizes $\left|\left(r_p^2+r_s^2e^{i2\varphi}\right)\right|$. This is the arrangement we recently used to measure the longitudinal Kerr effect from a 42-nm Ni film with an OI ZA-SI.[15] It is easily seen that adding an arbitrary wave-plate with the fast axis along the y-axis works as well, and one may even choose φ other than 0 to further improve $\left|\left(r_p^2+r_s^2e^{i2\varphi}\right)\right|$, although the benefits are not significant.

To detect the transverse Kerr effect exclusively from the x_m-component of the magnetization (i.e., m_x), we add a quarter-wave plate (Wave plate #2 in Fig. 1) after the sample with its fast axis set at 45° from the x-axis. In this case, the optical arrangement is no longer invariant under the operation of $\sigma_v C_2 = C_2\sigma_v$ or σ_v' and we expect the contribution from the transverse Kerr effect. In this, the Jones matrix M becomes

$$M = \begin{bmatrix} 0 & r_s\left(r_p+\alpha_x m_x\right) \\ r_s\left(r_p-\alpha_x m_x\right) & 0 \end{bmatrix}. \quad (20)$$

With a general form of two orthogonally polarized states $P_1 = \begin{bmatrix} a \\ be^{i\varphi} \end{bmatrix}$ and $P_2 = \begin{bmatrix} b \\ -ae^{i\varphi} \end{bmatrix}$, we have

$$\alpha_K = \frac{1}{(b^2-a^2)}\mathrm{Im}\left\{\frac{2\alpha_x m_x}{r_p}\right\}, \quad (21)$$

$$I(\Omega) \sim \left|r_p r_s\right|^2(b^2-a^2)\times \mathrm{Im}\left\{\frac{2\alpha_x m_x}{r_p}\right\}. \quad (22)$$

The optimal choice for measuring the transverse Kerr effect is either $a=1$ and $b=0$ or vice versa, namely, $P_1 = \begin{bmatrix} 1 \\ 0 \end{bmatrix}$ and $P_2 = \begin{bmatrix} 0 \\ 1 \end{bmatrix}$. In fact, this is the equivalent of a zero loop-area

Sagnac interferometer to the situation in a finite loop-area Sagnac interferometer where P_1 and P_2, for two counter-propagating beams coming from the opposite sides of the magnetized sample, are both p-polarized and by symmetry only the transverse Kerr effect contributes to the differential phase as reported by Dodge *et al.*[16] In the present OI ZA-SI, the quarter-wave plate serves to turn the s-polarized backward-propagating beam into a p-polarized beam while the p-polarized forward-propagating beam into an s-polarized beam after the first reflection but before the second reflection off the sample. As a result, the two beams sense the reflection matrix [Eqs. (8) and (9)] but from the opposite directions as the p-polarized light.

We note that imperfections in optical elements along the Sagnac loop such as wave plates, objectives, and the sample alters the Jones matrix M from what we have presented in this section. They tend to mix contributions from the three magnetization components at ratios somewhat different from what we described, depending upon the extent of imperfection.

IV. EXPERIMENTAL DEMONSTRATION

A. Detection of longitudinal and transverse Kerr effects due to in-plane magnetization in a 32-nm Co film

To examine the findings of Sec. II, we measured the Kerr effect from a 32-nm Co film in the presence of an applied magnetic field using different optical arrangements of the OI ZA-SI as we discussed in Sec. III B. The Co film has an easy axis of magnetization in the plane of the film. We use an electromagnet to produce a variable magnetic field up to 1850 Oe. The latter is not strong enough to magnetize the Co film along the z_m-axis (perpendicular to the film surface). As a result, we only apply a magnetic field along the y_m-axis or the x_m-axis and observe the longitudinal Kerr effect due to m_y and the transverse Kerr effect due to m_x.

As shown in Fig. 1, we use a linearly polarized, collimated broadband light source centered at 780 nm with a full bandwidth of 30 nm and an initial power of 1 mW (QPhotonics, Ann Arbor, MI). The electro-optic modulator (EOM) is a $LiNbO_3$ phase modulator with V_π = 1.3 V (EOSPACE Inc., Redmond, WA). We apply a sinusoidal wave form to the EOM with an amplitude of 0.35 V and a time frequency f = 4.445 MHz (the angular frequency $\Omega = 2\pi f$ = 2.7915 $\times 10^7$ rad/s). This adds a phase shift $\Phi(t) = \Phi_0 \cos(\Omega t)$ to the TM component of the beam with Φ_0 = 0.85 rad. After being collimated with a 10× objective, the phase modulated beam has two polarized components $P_{10} = e^{i\Phi(t)}\begin{bmatrix}1\\0\end{bmatrix}$ (the p-polarized) and $P_{20} = \begin{bmatrix}0\\1\end{bmatrix}$ (the s-polarized). The beam passes through Wave plate #1 so that the two orthogonally polarized components are $P_1 = \begin{bmatrix}a\\be^{i\varphi}\end{bmatrix}$ and $P_2 = \begin{bmatrix}b\\-ae^{i\varphi}\end{bmatrix}$ (with $\sqrt{a^2+b^2}=1$) which emerge and form initial states of the two "counter-propagating beams" for the zero loop-area Sagnac interferometer. The beam is incident on the sample at 50°. When the beam returns after passing through Wave plate #2 (if present) twice, it passes through Wave plate #1 again, then the PM-fiber-EOM assembly, and finally the linear polarizer. A portion of the returning beam with an average power γI_{inc} = 2 μW is sent to the photo-receiver with the amplitude of the electric field

$$S(t) \sim \left[\left(P_2^\dagger M P_1\right) e^{i(\Phi(t)+\delta_{12})} + \left(P_1^\dagger M P_2\right) e^{i(\Phi(t+\tau)+\delta_{21})} + \text{terms of other arrival times}\right], \quad (23)$$

where τ is the round-trip time it takes the beam to traverse from EOM through the 10-m fiber and optical elements that follow including the sample and return back to EOM. The terms of other arrival times are contributions from reflection of the primary beams at various surfaces of the optical elements along the loop-wise optical path starting from the beam splitter and from the transmitted beams but along "paths" with different refractive indices, as elaborated in details by Fried *et al.*[13] These terms do not interfere with the first two terms in Eq. (23) and thus only add to the dc background of the photocurrent. The time frequency f = 4.445 MHz is chosen to make $\Omega\tau = 2\pi f\tau = \pi$ so that $\Phi(t+\tau) = -\Phi(t)$. δ_{12} and δ_{21} are the reciprocal phases acquired by the forward-traveling beam (P_1) and the backward-traveling beam (P_2) starting right after the EOM, respectively. The photo-receiver is a 125 MHz photo-receiver (New Focus Model-1801 Newport, CA). The receiver has a gain of 4 × 10^4 V/A and a responsivity of 0.45 A/W at 780 nm. The optical power of the beam arriving at the photo-receiver varies with time as

$$I(t) = (\gamma/4)\, I_{inc} \left|\left(P_2^\dagger M P_1\right) e^{i(\Phi(t)+\delta_{12})} + \left(P_2^\dagger M P_1\right) e^{i(\Phi(t+\tau)+\delta_{21})}\right|^2. \quad (24)$$

The first and second harmonics in modulation frequency are given by

$$I(\Omega) = (\gamma/2)\, I_{inc}\left|P_2^\dagger M P_1\right|^2 J_1(2\Phi_0)\sin(\alpha_K + (\delta_{21}-\delta_{12})) \cong (\gamma/2)\, I_{inc}\left|P_2^\dagger M P_1\right|^2 J_1(2\Phi_0)(\alpha_K + \Delta\delta_{12}), \quad (25)$$

$$I(2\Omega) = (\gamma/2)\, I_{inc}\left|P_2^\dagger M P_1\right|^2 J_2(2\Phi_0)\cos(\alpha_K + (\delta_{21}-\delta_{12})) \cong (\gamma/2)\, I_{inc}\left|P_2^\dagger M P_1\right|^2 J_2(2\Phi_0). \quad (26)$$

They are measured with an SRS844 lock-in amplifier (Stanford Research Systems, Palo Alto, CA). The choice of $2\Phi_0$ = 1.7 rad maximizes $J_1(2\Phi_0)$ to 0.58 and yields $J_2(2\Phi_0)$ = 0.28. $\Delta\delta_{12}$ is the residual reciprocal phase difference acquired by the two "beams" as the Sagnac paths traversed by the two beams cannot be perfectly identical. In our present interferometer, it drifts slowly within ±7 μrad over 15 h. α_K is a function of the sample magnetization given by Eq. (2). It is determined experimentally from the ratio of the first harmonic $I(\Omega)$ to the second harmonic $I(2\Omega)$ through Eqs. (4), (25) and (26).

To compare the signal-to-noise ratio of different arrangements for measuring longitudinal Kerr effects, we measured the longitudinal Kerr rotation from the 32-nm Co film induced by an external magnetic field using four optical arrangements as described by Eqs. (12)–(19) in Sec. III B. The reflectivities of Co at an incidence angle of 50° are $r_p \cong 0.67 + i0.34$ and $r_s = -0.87 - i0.17$.[18] When the amplifier noise in the photo-receiver dominates, we expect the arrangement that yields the largest $I(\Omega)$ to have the highest signal-to-noise ratio. If the variation in $\Delta\delta_{12}$ dominates the "noise" in the measurement of α_K, we expect the arrangement that yields the largest α_K to be optimal. We found that the former was the case.

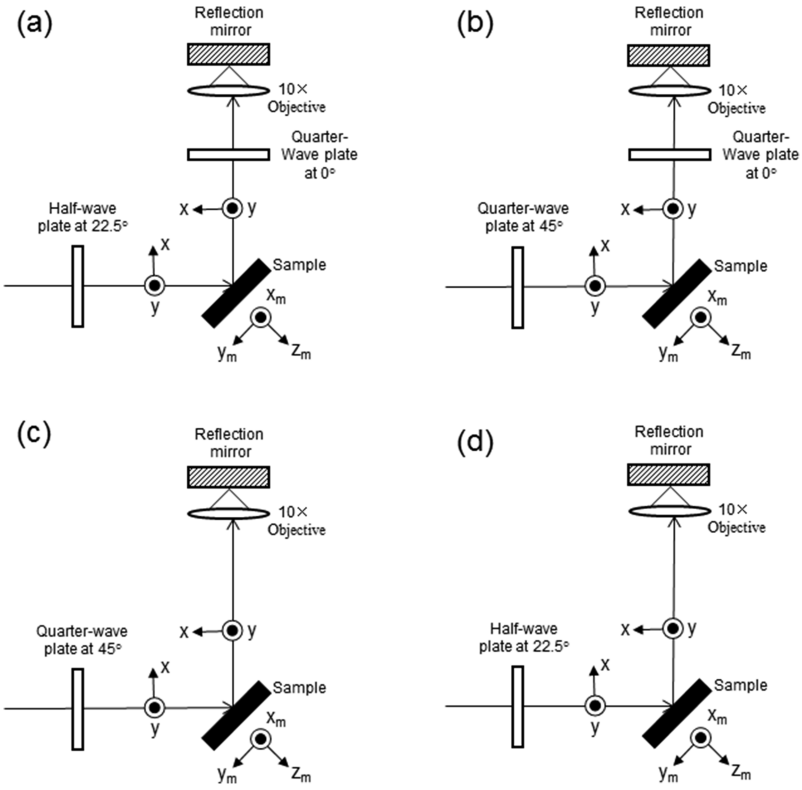

FIG. 2. Four arrangements for the part beyond the second 10× objective in Fig. 1 of the zero loop-area Sagnac interferometer for measuring longitudinal and polar Kerr rotation from a magnetized sample.

The first arrangement is in Fig. 2(a) with $P_1 = \frac{1}{\sqrt{2}}\begin{bmatrix}1\\1\end{bmatrix}$ and $P_2 = \frac{1}{\sqrt{2}}\begin{bmatrix}1\\-1\end{bmatrix}$ and M given by Eq. (17) so that the longitudinal Kerr rotation is given by Eq. (18) with $\alpha_K = 2\theta_{K,L} = \mathrm{Im}\left\{\frac{4\alpha_y m_y (r_p - r_s)}{r_p^2 + r_s^2}\right\}$ and $I(\Omega) \sim \left|\left(r_p^2 + r_s^2\right)\left(r_p - r_s\right)\right|$ by Eq. (19) with $\varphi = 0$.

The second arrangement is shown in Fig. 2(b) so that $P_1 = \frac{1}{\sqrt{2}}\begin{bmatrix}1\\i\end{bmatrix}$ and $P_2 = \frac{1}{\sqrt{2}}\begin{bmatrix}1\\-i\end{bmatrix}$ and M is again given by Eq. (17). In this case, $\alpha_K = 2\theta_{K,L} = \mathrm{Im}\left\{i\frac{4\alpha_y m_y (r_p - r_s)}{r_p^2 - r_s^2}\right\}$ also from Eq. (18) and $I(\Omega) \sim \left|\left(r_p^2 - r_s^2\right)\left(r_p - r_s\right)\right|$ again from Eq. (19) with $\varphi = \pi/2$.

The third arrangement is illustrated in Fig. 2(c) so that $P_1 = \frac{1}{\sqrt{2}}\begin{bmatrix}1\\i\end{bmatrix}$ and $P_2 = \frac{1}{\sqrt{2}}\begin{bmatrix}1\\-i\end{bmatrix}$ and M is given by Eq. (14). As a result, $\alpha_K = 2\theta_{K,L} = \mathrm{Im}\left\{i\frac{4\alpha_y m_y (r_p + r_s)}{(r_p^2 + r_s^2)}\right\}$ from Eq. (15) and $I(\Omega) \sim \left|\left(r_p^2 + r_s^2\right)\left(r_p + r_s\right)\right|$ from Eq. (16) with $\varphi = \pi/2$.

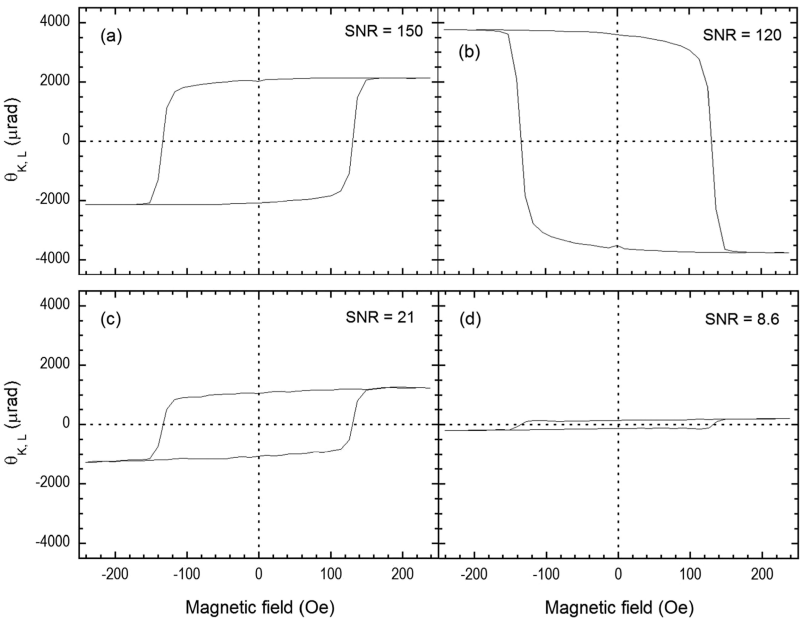

FIG. 3. Longitudinal Kerr rotation $\theta_{K,L} = \alpha_K/2$ from a 32-nm Co film, acquired using the zero loop-area Sagnac interferometer in four arrangements, vs. externally applied magnetic field along the y_m-axis. (a) $P_1 = \frac{1}{\sqrt{2}}\begin{bmatrix}1\\1\end{bmatrix}$ and $P_2 = \frac{1}{\sqrt{2}}\begin{bmatrix}1\\-1\end{bmatrix}$ and M is given by Eq. (17) [Fig. 2(a)]; (b) $P_1 = \frac{1}{\sqrt{2}}\begin{bmatrix}1\\i\end{bmatrix}$ and $P_2 = \frac{1}{\sqrt{2}}\begin{bmatrix}1\\-i\end{bmatrix}$ and M is again given by Eq. (17) [Fig. 2(b)]; (c) $P_1 = \frac{1}{\sqrt{2}}\begin{bmatrix}1\\i\end{bmatrix}$ and $P_2 = \frac{1}{\sqrt{2}}\begin{bmatrix}1\\-i\end{bmatrix}$ and M is given by Eq. (14) [Fig. 2(c)]; (d) $P_1 = \frac{1}{\sqrt{2}}\begin{bmatrix}1\\1\end{bmatrix}$ and $P_2 = \frac{1}{\sqrt{2}}\begin{bmatrix}1\\-1\end{bmatrix}$ and M is again given by Eq. (14) [Fig. 2(d)]. The standard deviation in each data point is obtained from 10 repeated measurements. The data are acquired with the lock-in amplifier time constant set to $\tau_{\text{Lock-in}} = 1$ s.

TABLE I. Longitudinal and transverse Kerr rotation $\theta_{K,L}$ and $\theta_{K,T}$ measured from a 32-nm Co film with five optical arrangements, the signal-to-noise ratio (SNR) (as defined in the main text), and factors in which magnitudes of $I(\Omega)$ and θ_K are proportional in different arrangements. The first four arrangements measure the longitudinal Kerr effect. The last one measures the transverse Kerr effect. Optimal arrangements for measuring Kerr rotation are highlighted in boldface.

	$I(\Omega)\propto$	$\theta_{K,L}\propto$	θ_K (μrad)	SNR
Figure 2(a)	$\left\|\left(\boldsymbol{r_p^2+r_s^2}\right)\left(\boldsymbol{r_p-r_s}\right)\right\|=2.1$	$\left\|\left(r_p-r_s\right)/\left(r_p^2+r_s^2\right)\right\|=1.24$	**2137**	**150**
Figure 2(b)	$\left\|\left(r_p^2-r_s^2\right)\left(r_p-r_s\right)\right\|=0.70$	$\left\|\left(r_p-r_s\right)/\left(r_p^2-r_s^2\right)\right\|=3.8$	3764	120
Figure 2(c)	$\left\|\left(r_p^2+r_s^2\right)\left(r_p+r_s\right)\right\|=0.35$	$\left\|\left(r_p+r_s\right)/\left(r_p^2+r_s^2\right)\right\|=0.20$	207	21
Figure 2(d)	$\left\|\left(r_p^2-r_s^2\right)\left(r_p+r_s\right)\right\|=0.11$	$\left\|\left(r_p+r_s\right)/\left(r_p^2-r_s^2\right)\right\|=0.61$	1259	9
Figure 4	$\boldsymbol{2\left\|r_p r_s^2\right\|}=1.2$	$\theta_{K,T}\propto\left\|1/2r_p\right\|=0.66$	**3652**	**190**

The fourth arrangement is illustrated in Fig. 2(d) so that $P_1=\frac{1}{\sqrt{2}}\begin{bmatrix}1\\1\end{bmatrix}$ and $P_2=\frac{1}{\sqrt{2}}\begin{bmatrix}1\\-1\end{bmatrix}$ and M is again given by Eq. (14). In this case, $\alpha_K=2\theta_{K,L}=\mathrm{Im}\left\{\frac{4\alpha_y m_y(r_p+r_s)}{(r_p^2-r_s^2)}\right\}$ also from Eq. (15) and $I(\Omega)\sim\left|\left(r_p^2-r_s^2\right)\left(r_p+r_s\right)\right|$ again from Eq. (16) with $\varphi=0$.

Figure 3 displays the longitudinal Kerr rotation $\theta_{K,L}=\alpha_K/2$ measured from the 32-nm Co film in the form of hysteresis loop using all four optical arrangements. The data are acquired in the single measurement with the lock-in amplifier time constant set at $\tau_{Lock\text{-}in}=1$ s. We take the ratio of the Kerr rotation measured at the zero magnetic field in the hysteresis loop to the standard deviation in Kerr rotation measured at the magnetic field at 250 G as the signal-to-noise ratio (SNR). Table I lists SNR's of the longitudinal Kerr rotation measurement for the four optical arrangements. We also list prefactors in which $I(\Omega)$ and α_K are, respectively, proportional to other than $\alpha_y m_y$. It is clear that the Kerr rotation is indeed proportional to the prefactor and has the largest value in the arrangement of Fig. 2(b) with $\left|\left(r_p-r_s\right)/\left(r_p^2-r_s^2\right)\right|=3.8$. Yet the SNR of the Kerr rotation measurement follows the magnitude of $I(\Omega)$ instead of α_K. The arrangement as illustrated with Fig. 2(a) yields the largest $I(\Omega)$ with $\left|\left(r_p^2+r_s^2\right)\left(r_p-r_s\right)\right|=2.1$ for a Co film and the largest SNR=150. This means that the noise of our present OI ZA-SI is dominated by the amplifier noise in the photo-receiver, not the temporal variation in the residual reciprocal phase difference.

To measure the transverse Kerr effect arising from the x_m component of the sample magnetization (i.e., $\alpha_x m_x$), we use another arrangement by removing the half-wave before the sample and setting the fast axis of the quarter-wave plate after the sample set to 45° from the x-axis as shown in Fig. 4. In this case, $P_1=\begin{bmatrix}1\\0\end{bmatrix}$ and $P_2=\begin{bmatrix}0\\1\end{bmatrix}$ and M is given by Eq. (20), and $I(\Omega)\propto 2|r_p r_s^2|$ from Eq. (21) and $\alpha_{K,T}=2\theta_{K,T}=\mathrm{Im}\left\{\frac{2\alpha_x m_x}{r_p}\right\}\propto|1/2r_p|$ from Eq. (22). We display in Fig. 5 the transverse Kerr rotation $\theta_{K,T}=\alpha_{K,T}/2$ measured from the Co film with the magnetic field applied along the x_m-axis (perpendicular to the plane of incidence). The data are again acquired in the single measurement with the lock-in amplifier time constant set at $\tau_{Lock\text{-}in}=1$ s. The magnitude of $\alpha_{K,T}$ and SNR are listed in the last row of Table I for comparison. These values of the longitudinal Kerr rotation for Co are consistent with the value reported by Qiu and Bader,[5] after considering the fact that the value in their report was measured with a different prefactor (the combination of reflectivity coefficients) from those listed in Column 3 of Table I.

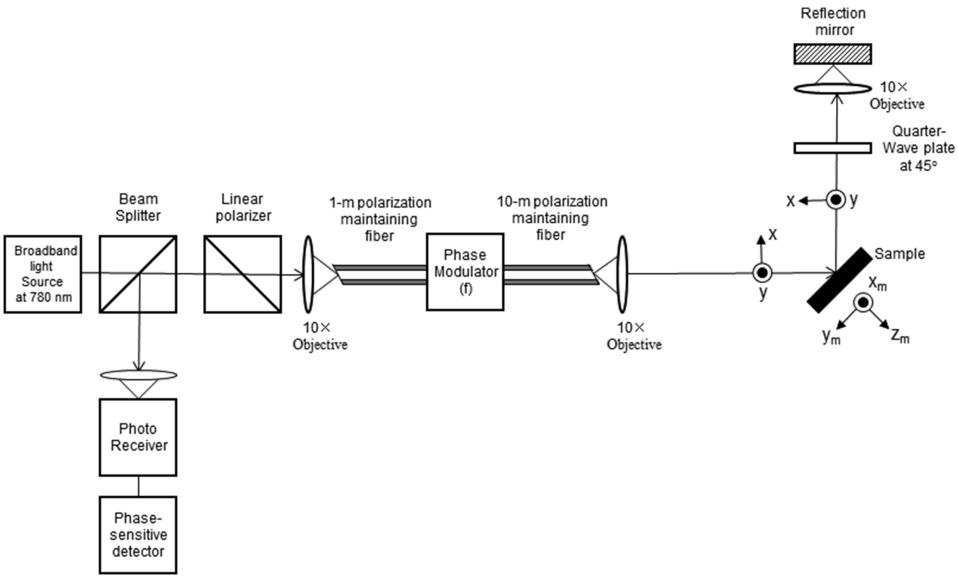

FIG. 4. The arrangement of the zero loop-area Sagnac interferometer for measuring the transverse Kerr effect of a magnetized sample. In this case, $P_1=\begin{bmatrix}1\\0\end{bmatrix}$ and $P_2=\begin{bmatrix}0\\1\end{bmatrix}$ and M is given by Eq. (20).

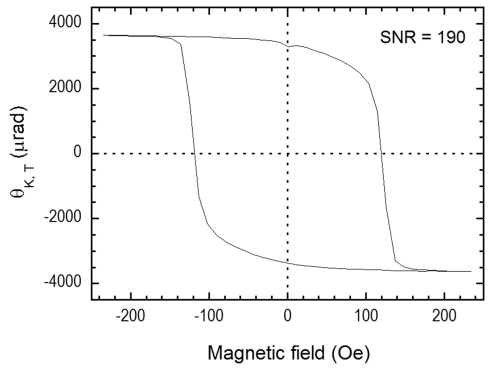

FIG. 5. Transverse Kerr rotation $\theta_{K,T} = \alpha_{K,T}/2$ from a 32-nm Co film vs. applied magnetic field, acquired with the arrangement illustrated in Fig. 4. The external field is applied along the x_m-axis parallel to the film surface.

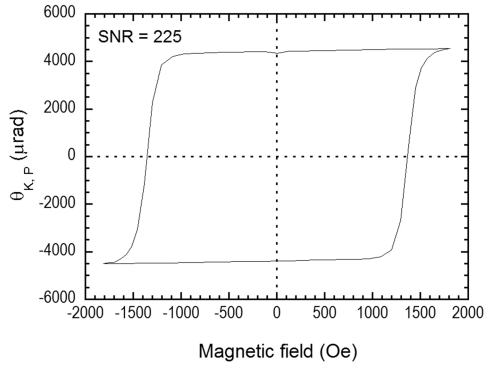

FIG. 6. Polar Kerr rotation $\theta_{K,P} = \alpha_{K,P}/2$ from a 12-nm film of (3 Å-Co/9 Å-Pd)$_{10}$, measured with the optical arrangement shown in Fig. 2(c), vs. externally applied magnetic field along the z_m-axis perpendicular to the film surface. In this case, $P_1 = \frac{1}{\sqrt{2}}\begin{bmatrix}1\\ i\end{bmatrix}$ and $P_2 = \frac{1}{\sqrt{2}}\begin{bmatrix}1\\ -i\end{bmatrix}$ and M is given by Eq. (14).

B. Detection of polar Kerr effect from a [3 Å-Co/9 Å-Pd]$_{10}$ film

To further illustrate the utility of an OI ZA-SI for detecting polar Kerr effects, we measured the Kerr effect from a [3 Å-Co/9 Å-Pd]$_{10}$ film grown on Si due to an external magnetic field applied perpendicular to the film surface. The film has an easy axis along the z_m-axis. A separate magnetic measurement shows that the coercive field of the [3 Å-Co/9 Å-Pd]$_{10}$ film is ~1300 Oe, within the range of our electromagnet with a pole gap of 2.5 cm. We performed the measurement using all four arrangements as illustrated in Fig. 2.

The arrangement shown in Fig. 2(a) has $P_1 = \frac{1}{\sqrt{2}}\begin{bmatrix}1\\ 1\end{bmatrix}$ and $P_2 = \frac{1}{\sqrt{2}}\begin{bmatrix}1\\ -1\end{bmatrix}$ and M is given by Eq. (17). It yields the polar Kerr rotation from Eq. (18) as $\alpha_K = 2\theta_{K,P} = \mathrm{Im}\left\{\frac{4\alpha_z m_z (r_p + r_s)}{r_p^2 + r_s^2}\right\}$ and $I(\Omega) \sim \left|\left(r_p^2 + r_s^2\right)\left(r_p + r_s\right)\right|$ by Eq. (19) with $\varphi = 0$. The arrangement in Fig. 2(b) has $P_1 = \frac{1}{\sqrt{2}}\begin{bmatrix}1\\ i\end{bmatrix}$ and $P_2 = \frac{1}{\sqrt{2}}\begin{bmatrix}1\\ -i\end{bmatrix}$ and is M again given by Eq. (17) and yields $\alpha_K = 2\theta_{K,P} = \mathrm{Im}\left\{i\frac{4\alpha_z m_z (r_p + r_s)}{r_p^2 - r_s^2}\right\}$ from Eq. (18) and $I(\Omega) \sim \left|\left(r_p^2 - r_s^2\right)\left(r_p + r_s\right)\right|$ from Eq. (19) with $\varphi = \pi/2$. The arrangement in Fig. 2(c) has $P_1 = \frac{1}{\sqrt{2}}\begin{bmatrix}1\\ i\end{bmatrix}$ and $P_2 = \frac{1}{\sqrt{2}}\begin{bmatrix}1\\ -i\end{bmatrix}$ and M is given by Eq. (14) and leads to $\alpha_K = 2\theta_{K,P} = \mathrm{Im}\left\{i\frac{4\alpha_z m_z (r_p - r_s)}{(r_p^2 + r_s^2)}\right\}$ from Eq. (15) and $I(\Omega) \sim \left|\left(r_p^2 + r_s^2\right)\left(r_p - r_s\right)\right|$ from Eq. (16) with $\varphi = \pi/2$. The arrangement in Fig. 2(d) has $P_1 = \frac{1}{\sqrt{2}}\begin{bmatrix}1\\ 1\end{bmatrix}$ and $P_2 = \frac{1}{\sqrt{2}}\begin{bmatrix}1\\ -1\end{bmatrix}$ and M is again given by Eq. (14). It yields $\alpha_K = 2\theta_{K,P} = \mathrm{Im}\left\{\frac{4\alpha_z m_z (r_p - r_s)}{(r_p^2 - r_s^2)}\right\}$ from Eq. (15) and $I(\Omega) \sim \left|\left(r_p^2 - r_s^2\right)\left(r_p - r_s\right)\right|$ from Eq. (16) with $\varphi = 0$.

Figure 6 shows the hysteresis loop measured with the arrangement illustrated in Fig. 2(c). It yields the second largest polar Kerr rotation (4500 μrad) but with the highest signal-to-noise ratio (SNR = 225), among the four arrangements, as expected. Table II lists SNR's of Kerr rotation measurements in all four optical arrangements and prefactors that $I(\Omega)$ and α_K are proportional to, respectively. The amplitude of the Kerr rotation has the largest value when measured with the arrangement of Fig. 2(d). Yet the SNR of the Kerr rotation measurement follows the magnitude of $I(\Omega)$ instead. It once again shows that in our present OI ZA-SI, the noise is dominated by the amplifier noise of the photo-receiver, not the temporal variation in the residual reciprocal phase difference.

The reversal of the magnetization in the [3 Å-Co/9 Å-Pd]$_{10}$ multilayer film induced by reversing the applied magnetic field along the z_m-axis is accompanied by a coherent rotation for a noticeable portion of the sample. To see this, we measured the transverse Kerr rotation using the arrangement of Fig. 4 while applying the external magnetic field only along the z_m-axis. The result is shown in Fig. 7.

TABLE II. Polar Kerr rotation $\theta_{K,P}$ measured from a [3 Å-Co/9 Å-Pd]$_{10}$ film with four optical arrangements, the signal-to-noise ratio (SNR) (as defined in the main text), and factors in which magnitudes of $I(\Omega)$ and $\theta_{K,P}$ are proportional in different arrangements. Since we do not have complex refractive indices for [3 Å-Co/9 Å-Pd]$_{10}$, we use the magnitude of the photocurrent $I(\Omega)$ normalized to the value for the arrangement of Fig. 2(c) for numerical values in the second column.

	$I(\Omega$, measured)$\propto$	$\theta_{K,P}\propto$	$\theta_{K,P}$ (μrad)	SNR
Figure 2(a)	$\left\|\left(r_p^2 + r_s^2\right)\left(r_p + r_s\right)\right\| \sim 0.24$	$\left\|\left(r_p + r_s\right) / \left(r_p^2 + r_s^2\right)\right\|$	950	73
Figure 2(b)	$\left\|\left(r_p^2 - r_s^2\right)\left(r_p + r_s\right)\right\| \sim 0.19$	$\left\|\left(r_p + r_s\right) / \left(r_p^2 - r_s^2\right)\right\|$	1432	57
Figure 2(c)	$\left\|\left(\mathbf{r_p^2 + r_s^2}\right)\left(\mathbf{r_p - r_s}\right)\right\| \sim \mathbf{1.0}$	$\left\|\left(r_p - r_s\right) / \left(r_p^2 + r_s^2\right)\right\|$	**4500**	**225**
Figure 2(d)	$\left\|\left(r_p^2 - r_s^2\right)\left(r_p - r_s\right)\right\| \sim 0.27$	$\left\|\left(r_p - r_s\right) / \left(r_p^2 - r_s^2\right)\right\|$	4860	70

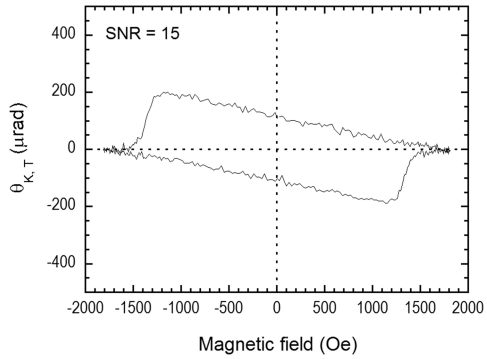

FIG. 7. Transverse Kerr rotation $\theta_{K,T} = \alpha_{K,T}/2$ from the (3 Å-Co/9 Å-Pd)$_{10}$ film vs. applied magnetic field along the z_m-axis, using the arrangement shown in Fig. 4. In this case, $P_1 = \begin{bmatrix}1\\0\end{bmatrix}$ and $P_2 = \begin{bmatrix}0\\1\end{bmatrix}$ and M is given by Eq. (20). This indicates that the hysteresis loop in Fig. 6 is accompanied by a coherent rotation of a portion of the magnetization through the film surface plane.

V. DISCUSSION

We showed once again that a zero loop-area Sagnac interferometer reveals the time-reversal symmetry breaking (TRSB) effect, while efficiently suppressing otherwise overwhelming birefringent effects along the Sagnac loop.[12,13] More importantly, we have demonstrated in this work that the introduction of the oblique-incidence geometry to such an interferometer enables the detection of the TRSB effect from an *arbitrarily oriented* magnetization of a sample in the loop. In addition, the oblique-incidence geometry affords five optical arrangements as illustrated in Figs. 2 and 4 that take the full advantage of crystal symmetry operations, instead of just one for a normal-incidence zero loop-area Sagnac interferometer.[12,13] These symmetry operations interchange the "source" and the "detector" and transform the polarization state of the forward-propagating beam to the polarization state of the backward-propagating state.[17] As a result, we have the option to choose one from these five arrangements to predominantly measure the Kerr effect from one Cartesian component of the sample magnetization with the highest signal-to-noise ratio while minimizing effects from the other two Cartesian components as illustrated in Fig. 3. Depending upon the dominant source of noise in the measurement of the Kerr rotation, one may choose the arrangement that yields the largest Kerr rotation angle or the one that yields the largest photocurrent at the first harmonic of the EOM modulation frequency. Using three different arrangements, one can measure the Kerr rotation from all three Cartesian components of a sample magnetization with nearly equally high signal-to-noise ratio as summarized in Tables I and II. If the complex refractive index is known precisely, the ratio between the longitudinal and polar Kerr rotations can be determined in each of the four arrangements in Fig. 2 by performing measurements using these four arrangements and solving for separate contributions from the longitudinal Kerr effect and polar Kerr effect. The numerical accuracy of such determination is often not good. A more practical, accurate way of finding the ratio between the longitudinal and polar Kerr rotations is to apply a sufficiently large magnetic field to saturate the magnetization along the z-axis so that only the polar Kerr effect is at work. The sign and amplitude of the differential phase with the sample magnetization saturated along the z-axis are recorded for one calibration value. One repeats the process by applying a sufficient large magnetic field to saturate the magnetization along the y-axis so that only the longitudinal Kerr effect is at work. The sign and amplitude of the differential phase with the sample magnetization saturated along the y-axis are recorded as the second calibration value. One then expresses the differential phase in general as a function of the tilt angle of the sample magnetization and these two calibration values. In this way, not only one can determine the ratio between the longitudinal and polar Kerr rotations in each of the four arrangements in Fig. 2, one can also find the tilt angle of the sample magnetization, all done without having to know refractive indices of the sample.

As to the sensitivity of our present OI ZA-SI, we note that the noise (the standard deviation of the measured Kerr rotation) is dominated by the amplifier noise in the photo-receiver. The input noise equivalent power of a 125 MHz photo-receiver (New Focus Model-1801 Newport, CA) is specified to be $NEP = 3.3\,\text{pW}/\sqrt{\text{Hz}}$. With a lock-in amplifier time constant set at $\tau_{Lock\text{-}in} = 1$ s, the noise power is $I_n = 3.3$ pW. This means that the amplifier noise in the Kerr rotation measurement is $\delta\theta_K = I_n/((\gamma/2)I_{inc}J_1(2\Phi_0)) = 7\ \mu$rad, close to what we observed in the present study. Since the photo-receiver can take as much as 110 μW, by simply increasing the optical power returned to the receiver γI_{inc} to this level, we will be able to decrease the minimum detectable Kerr rotation of the present OI ZA-SI to $1.3 \times 10^{-7}\,\text{rad}/\sqrt{\text{Hz}}$. If we can use the photo-receiver with an $NEP = 0.5\,\text{pW}/\sqrt{\text{Hz}}$, the minimum detectable Kerr rotation will be $2 \times 10^{-8}\,\text{rad}/\sqrt{\text{Hz}}$. We should point out that at these low levels of amplifier noise, the drift in the residual reciprocal phase difference $\Delta\delta_{12}$ and the photo shot noise need to be considered and dealt with.

Compared to oblique incidence finite loop-area Sagnac interferometers that also measure Kerr rotation from all three components of magnetization,[16] a zero loop-area Sagnac interferometer employs two orthogonally polarized components of a single optical beam for "the two counter-propagating beams" instead of two separate beams for interferometry. As a result, it is comparatively easy to ensure that the two "beams" traverse the same Sagnac path by avoiding beam splitting and beam recombination and to make the signal much less subject to residual movements of the sample and elements in the Sagnac loop. Since a normal-incidence oblique-incidence Sagnac interferometry only measures polar Kerr effects, whereas an oblique-incidence Sagnac interferometry measures Kerr effects (longitudinal, transverse, and polar) from all three components of magnetization in a sample, our present work expands the promise of the zero loop-area Sagnac interferometry proposed by Xia and co-workers.[12]

Finally, we revisit constraints of time-reversal symmetry on the effect of optical elements other than the sample of interest. An oblique-incidence zero loop-area Sagnac interferometer makes it possible to study a magnetized sample without bringing optical elements to close proximity of the sample. For such a sensing application, optical beams have to pass through additional transmitting elements such as optical windows or extra fibers. The latter typically have significant birefringence due to strain or stress in the window or fiber

materials. It would seem that they might render the Sagnac interferometer ineffective. Yet as long as the effects of these windows or fibers preserve the time-reversal symmetry, their Jones matrices will satisfy the general requirement specified in Eqs. (5)–(7). As a result, they only affect the overall magnitude of the Kerr rotation and relative contributions from three components of the sample magnetization. If the sample is nonmagnetic, addition of these windows or extra optical fibers will not change $m_{21} = m_{12}$ as it is demanded by TRS. In practice, they can only contribute to the background through the residual reciprocal phase difference $\Delta\delta_{12}$. For the same reason, the surface morphology of a sample such as roughness and the presence of dust does not break time-reversal symmetry and thus has no effect on the differential phase as determined with Eq. (4).

VI. CONCLUSION

We described a zero loop-area Sagnac interferometer in which optical beams interact with the sample at oblique incidence so that Kerr effects from an arbitrarily oriented magnetization in a sample can be characterized. By considering crystal symmetries allowed in such an interferometer, we identified optimal arrangements for measuring longitudinal, transverse, and polar Kerr effects with equally high signal-to-noise ratios. At present, the minimum detectable Kerr rotation is only limited by the amplifier noise in the photo-receiver. By improving the optical power reaching the receiver to ~110 μW, the minimum detectable Kerr rotation can be as low as $1.3 \times 10^{-7}\,\mathrm{rad}/\sqrt{\mathrm{Hz}}$. The simplicity and the folded Sagnac path render such an interferometer inherently stable and thus having a high sensitivity to time-reversal breaking effects in a sample as already illustrated in normal-incidence zero loop-area Sagnac interferometers by Xia *et al.* and Fried *et al.*[12–14]

ACKNOWLEDGMENTS

X.D.Z. wishes to thank Galina Malovichko for assistance in data collection and processing.

[1] N. A. Spaldin and M. Fiebig, Science **309**, 391 (2005).
[2] W. Eerenstein, N. D. Mathur, and J. F. Scott, Nature **442**, 759 (2006).
[3] J. A. Mundy *et al.*, Nature **537**, 523 (2016).
[4] R. P. Hunt, J. Appl. Phys. **38**, 1652 (1967).
[5] Z. Q. Qiu and S. D. Bader, Rev. Sci. Instrum. **71**, 1243 (2000).
[6] Z. Q. Qiu and S. D. Bader, J. Magn. Magn. Mater. **200**, 664 (1999).
[7] Y. K. Kato, R. C. Myers, A. C. Gossard, and D. D. Awshalom, Science **306**, 1910 (2004).
[8] S. Spielman, K. Fesler, C. B. Eom, T. H. Geballe, M. M. Fejer, and A. Kapitulnik, Phys. Rev. Lett. **65**, 123 (1990).
[9] S. Spielman, J. S. Dodge, L. W. Lombardo, C. B. Eom, M. M. Fejer, T. H. Geballe, and A. Kapitulnik, Phys. Rev. Lett. **68**, 3472 (1992).
[10] E. R. Schemm, W. J. Gannon, C. M. Wishne, W. P. Halperin, and A. Kapitulnik, Science **345**, 190 (2014).
[11] A. Kapitulnik, J. S. Dodge, and M. M. Fejer, J. Appl. Phys. **75**, 6872 (1994).
[12] J. Xia, P. T. Beyersdorf, M. M. Fejer, and A. Kapitulnik, Appl. Phys. Lett. **89**, 062508 (2006).
[13] A. Fried, M. Fejer, and A. Kapitulnik, Rev. Sci. Instrum. **85**, 103707 (2014).
[14] J. Xia, Ph.D. thesis, Stanford University, 2008.
[15] X. D. Zhu and G. Malovichko, AIP Adv. **7**, 055008 (2017).
[16] J. S. Dodge, L. Klein, M. M. Fejer, and A. Kapitulnik, J. Appl. Phys. **79**, 6186 (1996).
[17] A. L. Shelankov and G. E. Pikus, Phys. Rev. B. **46**, 3326 (1992).
[18] J. H. Weaver and H. P. R. Frederikse, in *Optical Properties of Selected Elements*, CRC Handbook of Chemistry and Physics, 84th ed., edited by D. R. Lide (CRC Press, Boca Raton, 2004), pp. 12–135.